Earth and Planetary Science Letters 553 (2021) 116657

Contents lists available at ScienceDirect

Earth and Planetary Science Letters

www.elsevier.com/locate/epsl

Miocene to present oceanographic variability in the Scotia Sea and Antarctic ice sheets dynamics: Insight from revised seismic-stratigraphy following IODP Expedition 382

Lara F. Pérez [a,*], Yasmina M. Martos [b,c], Marga García [d], Michael E. Weber [e], Maureen E. Raymo [f], Trevor Williams [g], Fernando Bohoyo [h], Linda Armbrecht [i], Ian Bailey [j], Stefanie Brachfeld [k], Anna Glüder [l], Michelle Guitard [m], Marcus Gutjahr [n], Sidney Hemming [f], Iván Hernández-Almeida [o], Frida S. Hoem [p], Yuji Kato [q], Suzanne O'Connell [r], Victoria L. Peck [a], Brendan Reilly [s], Thomas A. Ronge [t], Lisa Tauxe [s], Jonathan Warnock [u], Xufeng Zheng [v], and the IODP Expedition 382 Scientists [g]

[a] British Antarctic Survey, Cambridge, UK
[b] NASA Goddard Space Flight Center, Greenbelt, MD, USA
[c] University of Maryland, College Park, MD, USA
[d] Spanish Institute of Oceanography, Cádiz, Spain
[e] University of Bonn, Bonn, Germany
[f] Lamont-Doherty Earth Observatory of Columbia University, Palisades, NY, USA
[g] International Ocean Discovery Program/Texas A&M University, College Station, TX, USA
[h] Geological Survey of Spain, Madrid, Spain
[i] School of Biological Sciences, University of Adelaide, Australia
[j] Camborne School of Mines, College of Engineering, Mathematics & Physical Sciences, University of Exeter, Penryn, UK
[k] Earth and Environmental Studies Montclair State University, Montclair, NJ, USA
[l] College of Earth, Ocean and Atmospheric Sciences, Oregon State University, Corvallis, OR, USA
[m] College of Marine Science, University of South Florida, St. Petersburg, FL, USA
[n] GEOMAR Helmholtz Centre for Ocean Research, Kiel, Germany
[o] Department of Earth Sciences, ETH, Zurich, Switzerland
[p] Department of Earth Sciences, Utrecht University, Utrecht, Netherlands
[q] Center for Advanced Marine Core Research, Kochi University, Kochi, Japan
[r] Department of Earth and Environmental Sciences, Wesleyan University, Middletown, CT, USA
[s] Scripps Institution of Oceanography, University of California, San Diego, CA, USA
[t] Alfred Wegener Institute Helmholtz-Center for Polar and Marine Research, Bremerhaven, Germany
[u] Indiana University of Pennsylvania, Indiana, PA, USA
[v] Chinese Academy of Sciences, South China Sea Institute of Oceanology, Guangzhou, China

ARTICLE INFO

Article history:
Received 18 May 2020
Received in revised form 5 October 2020
Accepted 30 October 2020
Available online 19 November 2020
Editor: J.-P. Avouac

Keywords:
Drake Passage
Scotia Sea
IODP Expedition 382

ABSTRACT

Scotia Sea and the Drake Passage is key towards understanding the development of modern oceanic circulation patterns and their implications for ice sheet growth and decay. The sedimentary record of the southern Scotia Sea basins documents the regional tectonic, oceanographic and climatic evolution since the Eocene. However, a lack of accurate age estimations has prevented the calibration of the reconstructed history. The upper sedimentary record of the Scotia Sea was scientifically drilled for the first time in 2019 during International Ocean Discovery Program (IODP) Expedition 382, recovering sediments down to ~643 and 676 m below sea floor in the Dove and Pirie basins respectively. Here, we report newly acquired high resolution physical properties data and the first accurate age constraints for the seismic sequences of the upper sedimentary record of the Scotia Sea to the late Miocene. The drilled record contains four basin-wide reflectors – Reflector-c, -b, -a and -a' previously estimated to be ~12.6 Ma,

* Corresponding author.
E-mail addresses: larrez@bas.ac.uk (L.F. Pérez), yasmina.martos@nasa.gov (Y.M. Martos), marga.garcia@ieo.es (M. García), mike.weber@uni-bonn.de (M.E. Weber), raymo@ldeo.columbia.edu (M.E. Raymo), williams@iodp.tamu.edu (T. Williams), f.bohoyo@igme.es (F. Bohoyo), linda.armbrecht@adelaide.edu.au (L. Armbrecht), I.Bailey@exeter.ac.uk (I. Bailey), brachfelds@mail.montclair.edu (S. Brachfeld), gluedera@oregonstate.edu (A. Glüder), mguitard@mail.usf.edu (M. Guitard), mgutjahr@geomar.de (M. Gutjahr), sidney@ldeo.columbia.edu (S. Hemming), ivan.hernandez@erdw.ethz.ch (I. Hernández-Almeida), f.s.hoem@uu.nl (F.S. Hoem), jm-ykato@kochi-u.ac.jp (Y. Kato), soconnell@wesleyan.edu (S. O'Connell), vlp@bas.ac.uk (V.L. Peck), btreilly@ucsd.edu (B. Reilly), tronge@awi.de (T.A. Ronge), ltauxe@ucsd.edu (L. Tauxe), jwarnock@iup.edu (J. Warnock), zxf@scsio.ac.cn (X. Zheng), expedition_382_participants@iodp.tamu.edu.

https://doi.org/10.1016/j.epsl.2020.116657

oceanic gateways
Antarctic ice sheets evolution
core-log-seismic correlation

~6.4 Ma, ~3.8 Ma and ~2.6 Ma, respectively. By extrapolating our new Scotia Sea age model to previous morpho-structural and seismic-stratigraphic analyses of the wider region we found, however, that the four discontinuities drilled are much younger than previously thought. Reflector-c actually formed before 8.4 Ma, Reflector-b at ~4.5/3.7 Ma, Reflector-a at ~1.7 Ma, and Reflector-a' at ~0.4 Ma. Our updated age model of these discontinuities has major implications for their correlation with regional tectonic, oceanographic and cryospheric events. According to our results, the outflow of Antarctic Bottom Water to northern latitudes controlled the Antarctic Circumpolar Current flow from late Miocene. Subsequent variability of the Antarctic ice sheets has influenced the oceanic circulation pattern linked to major global climatic changes during early Pliocene, Mid-Pleistocene and the Marine Isotope Stage 11.

1. Introduction

The formation and evolution of the Tasmanian and Drake Passage-Scotia Sea gateways allowed for the establishment and history of the Antarctic Circumpolar Current (ACC). The onset of the ACC influenced the thermal isolation of Antarctica, that together with atmospheric CO_2 decline, enabled growth of the Antarctic ice sheets (e.g., Barker et al., 2007; Bijl et al., 2013). Formed during the final phases of the Gondwana breakup, the Drake Passage has since been a crucial area for exchange of water masses between the Pacific Ocean, the Atlantic Ocean and the Weddell Sea (e.g., Barker et al., 2007; Eagles and Jokat, 2014). The time of opening and establishment of deep-water circulation through the Drake Passage and Scotia Sea is still widely debated (e.g., Eagles and Jokat, 2014; Maldonado et al., 2014). Tectonic reconstructions based on age constraints from oceanic spreading magnetic anomalies and heat flow measurements point to divergence of the continental blocks starting around 41 Ma (e.g., Eagles and Jokat, 2014). While some palaeoceanographic reconstructions, based on variability of isotopic ratios, propose shallow flows across the Drake Passage existing since then (Scher and Martin, 2006), others however suggest a barrier to deep-water flows lasting until ~12 Ma (e.g., Dalziel et al., 2013).

The eastward migration of continental blocks, which initially maintained a continental bridge between South America and the Antarctic Peninsula, and the subsequent formation of oceanic crust by a number of spreading centres led to the formation of the Scotia Sea as a cluster of distinct sedimentary basins in a back-arc extensional context (e.g., Dalziel et al., 2013; Martos et al., 2014). A total of five sedimentary basins were emplaced within the southern Scotia Sea (Fig. 1). Since their formation, these sedimentary basins have impacted and recorded elements of the global oceanographic dynamics (e.g. Naveira-Garabato et al., 2002). Their bathymetry and morphology have controlled the flow of the deepest part of the ACC, the Lower Circumpolar Deep Water (LCDW), in turn modifying the Atlantic Meridional Overturning Circulation (AMOC). Between the Polar Front and the Southern ACC Front, modern South Pacific Deep Water (SPDW) has bathed the seafloor beneath the LCDW since the Pliocene (Kwiek and Ravelo, 1999). South of the Southern ACC Front, the deepest abyssal plains are bathed by Antarctic Bottom Water (AABW) which mixes with the LCDW (e.g., Naveira-Garabato et al., 2002). The flow of AABW has repeatedly waxed and waned, but it has connected the sedimentary basins of the Southern Hemisphere since the late Miocene (Carter and McCave, 1994). The southern Scotia Sea basins have acted as distinct oceanic gateways for the northward outflow of the Weddell Sea component of the AABW, the Weddell Sea Deep Water (WSDW) (e.g., Naveira-Garabato et al., 2002).

Several studies have dealt with the large-scale seismic-stratigraphic reconstruction of the southern Scotia Sea basins (Pérez et al., 2019 and references therein). The regional sedimentary stacking pattern has recorded the reorganization of the tectonic regime that modified the water masses distribution. Ultimately, these tectonic and oceanographic events were tentatively associated with climatic variations mainly related to glacial trends in the Southern and Northern hemispheres (e.g., Pérez et al., 2019). The main changes in the regional context have been largely described as major stratigraphic discontinuities identified and interpreted in the seismic record of the Scotia Sea (e.g., Maldonado et al., 2006, 2014; Martos et al., 2013; Pérez et al., 2019). Thus, the main regional change in the stratigraphic pattern is marked by Reflector-c (e.g., Maldonado et al., 2006). Above Reflector-c, three regional stratigraphic discontinuities have been defined in previous studies referred to as Reflector-b, Reflector-a and Reflector-a' (e.g., Maldonado et al., 2006; Martos et al., 2013; Pérez et al., 2017, 2019). The regional events represented by the stratigraphic discontinuities have been assumed to be time-synchronous across the southern Scotia Sea basins (e.g., Maldonado et al., 2006; Pérez et al., 2019). However, their estimated ages were necessarily based on assumptions of constant sedimentation rates over an underlying igneous crust, the age of which was assessed by spreading magnetic anomaly models (e.g., Eagles et al., 2006; Galindo-Zaldívar et al., 2006; Maldonado et al., 2006, 2014). Our study follows the previously established naming convention for the stratigraphic discontinuities implementing their age constrains.

The first scientific drilling of the Scotia Sea sedimentary record was performed during International Ocean Discovery Program (IODP) Expedition 382 in two of the southern Scotia Sea basins, Dove and Pirie (Fig. 1) (Weber et al., 2021). Sites U1536 and U1537 are located in the abyssal plain of Dove Basin at 3220 and 3713 m water depth, penetrating down to 643 and 349 m below seafloor (mbsf), respectively. Site U1538 was drilled in the northern part of Pirie Basin at 3131 m water depth and recovered sediment to 676 mbsf (Weber et al., 2021). All three sites reached Reflector-b (Figs. 2, 3, 4), therefore recovering the sedimentary record above this discontinuity, whereas only Site U1536 recovered sediments below Reflector-c (Fig. 2).

As the age constraints from IODP Expedition 382 paleomagnetic and biostratigraphic datums provide a well-developed age model, our objective here is to improve the age models for the previously established seismic-stratigraphy of the Scotia Sea overlying Reflector-c and relate them with coeval tectonic, oceanographic and cryospheric events. According to the new core-log-seismic correlation presented in this work, the major changes in the sedimentary stacking pattern of the southern Scotia Sea occurred after major variations in the prevailing regional oceanic circulation regime ultimately related to the late Miocene-Pleistocene climatic trends and Antarctic ice sheets dynamics.

2. Methods

2.1. Seismic data

A broad network of Multi- (MCS) and Single-channel Seismic (SCS) profiles exists over the southern Scotia Sea basins (Pérez et al., 2019). Of these, MCS profiles SCAN2004_SC10,

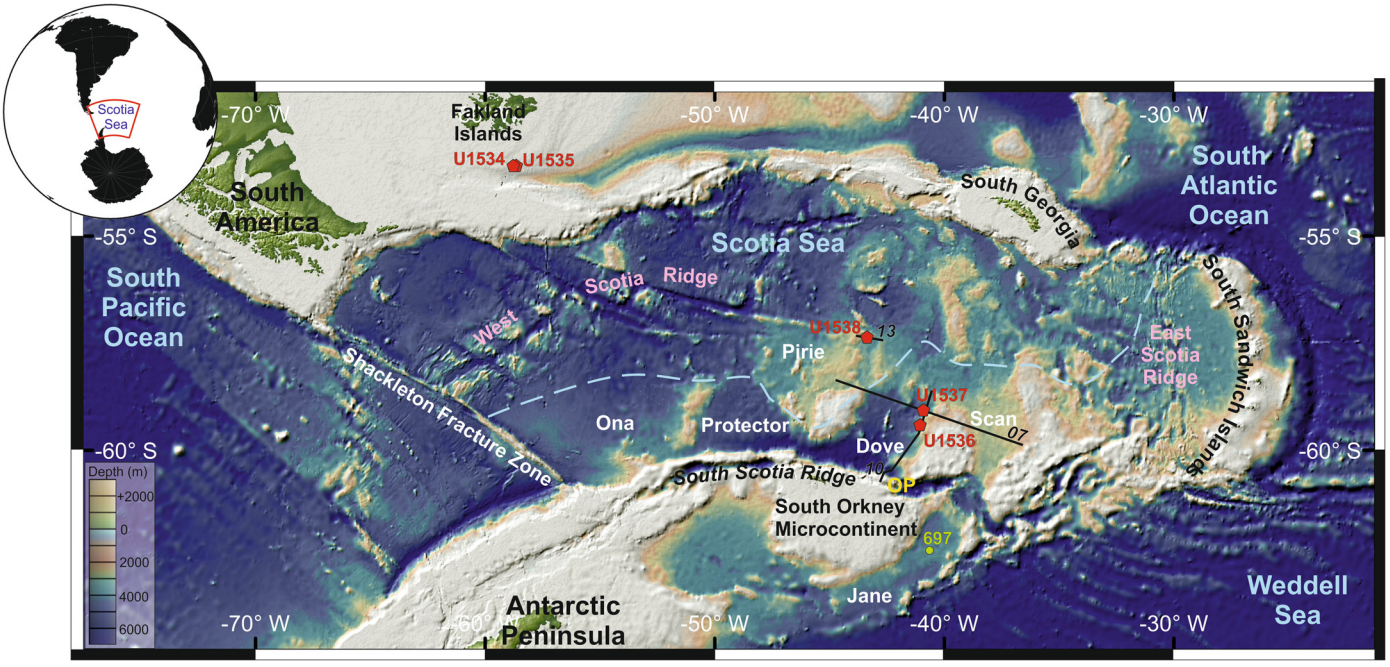

Fig. 1. Overview map of the Scotia Sea, bathymetry from Global Multi-Resolution Topography (GMRT) (Ryan et al., 2009). The names of the five southern Scotia Sea basins are highlighted. The red polygons mark the location of IODP Expedition 382 Sites. The green dot marks the location of ODP Site 697 from Leg 113. The location of the seismic profiles discussed in this work is marked in black as: 10, SCAN2004_SC10; 07, SCAN2004_SC07; and 13, SCAN2013_SC13. The dashed blue line marks the estimated present-day contact at the seafloor of Weddell Sea Deep Water (south of the contact), and South Pacific Deep Water (north of the contact), based on the South Antarctic Circumpolar Current Front. OP, Orkney Passage. (For interpretation of the colours in the figure(s), the reader is referred to the web version of this article.)

SCAN2004_SC07 and SCS profile SCAN2013_SC13 cross respectively over IODP Expedition 382 drilling Sites U1536, U1537 and U1538 (Fig. 1). SCAN2013 profile in Pirie Basin was acquired with an array of 2 Bolt airguns and a 3-channels streamer of 150 m length. The seismic signal was recorded through a DELPH-2 system and processed with Radex-Pro. Details on data acquisition and processing methods on the SCAN2004 profiles are given in Galindo-Zaldívar et al. (2006) and Pérez et al. (2014, 2017). Seismic interpretations presented in this work are based on previous publications in the area, i.e., Maldonado et al. (2006), Pérez et al. (2014, 2017, 2019).

2.2. Site data and core-log-seismic correlation

Three of the five sites drilled during IODP Expedition 382 are located in the Scotia Sea, Sites U1536, U1537 and U1538 (Fig. 1). Drilling and logging techniques are detailed in Weber et al. (2021). In this work, physical properties from wireline downhole (U1536) and core-log (U1536, U1537 and U1538) measurements are correlated with the seismic profiles to refine the interpretation of the upper sedimentary record of the Scotia Sea (Fig. 2, 3, 4).

Downhole measurements record in-situ conditions and are therefore considered the most accurate representation of the physical properties of the sedimentary record. The drill pipe occupied the uppermost 90 mbsf during logging, thus in the interval 0-90 mbsf only the natural gamma radiation downhole log is available. Below 90 mbsf, trends of wireline downhole and core-logged physical properties are similar at Site U1536 unless otherwise noted in the text (Fig. 2). The lack of downhole logging at Sites U1537 and U1538 limits the physical property values to the core logging measurements, although they can be approximately corrected to in-situ conditions based on the results from Site U1536. Compressional velocity is considered from core values measured in discrete samples with the P-wave caliper (PWC) and the downhole log at Site U1536. Velocity values derived from the P-wave core-logger (PWL) have large discrepancies due to cracks in the core liner or within the sediment, and are therefore not discussed in this work (Fig. 2B, 3B, 4B). Density values from moisture and density (MAD) samples generally match with the values obtained from the gamma-ray attenuation bulk densitometer (GRA) and the downhole density tool (RHOM). Magnetic susceptibility values from downhole measurements and the whole-core loop sensor are presented as unitless in instrument units (IU). Natural gamma radiation values were obtained from downhole and core logged measurements, and are presented in American Petroleum Institute (API) and counts per seconds (cps) units, respectively. Both physical properties have been resampled by running average to 5 m for the purpose of this work. Downhole formation resistivity logs were only obtained at Site U1536 (Fig. 2B).

A time-depth relationship was established during the expedition allowing correlation between borehole stratigraphy and seismic reflection features (Weber et al., 2021). Multiple models of time-depth correlation were explored based on the PWC and downhole logging values at Site U1536. Differences up to 40 m between downhole and PWC models in the lower part of Site U1536 are attributed to variations between in-situ measurements and values from expanded-sediments once the core adjusted to the laboratory conditions. Synthetic seismograms were created using the Petrel software package to select the best fit for the time-depth model. It should be noticed that the vertical resolution of the available seismic involves a depth uncertainty between 18 and 6 m as determined from the seismic wavelengths. Overall, the obtained core-log-seismic correlation provides the best possible tie between borehole data and seismic profiles, as supports the seismic signal fit with the acoustic impedance variability derived from the density and velocity logs (Fig. 2A, 3A, 4A). Only minor uncertainties (<2 m) are observed below 500 mbsf at Site U1536.

The age constraints presented in this work are based on the shipboard paleomagnetism and biostratigraphy (Table S1). The paleomagnetic age models were developed by measuring the natural remanent magnetization before and after alternating field demagnetization to 15 mT (Weber et al., 2021). Biostratigraphic

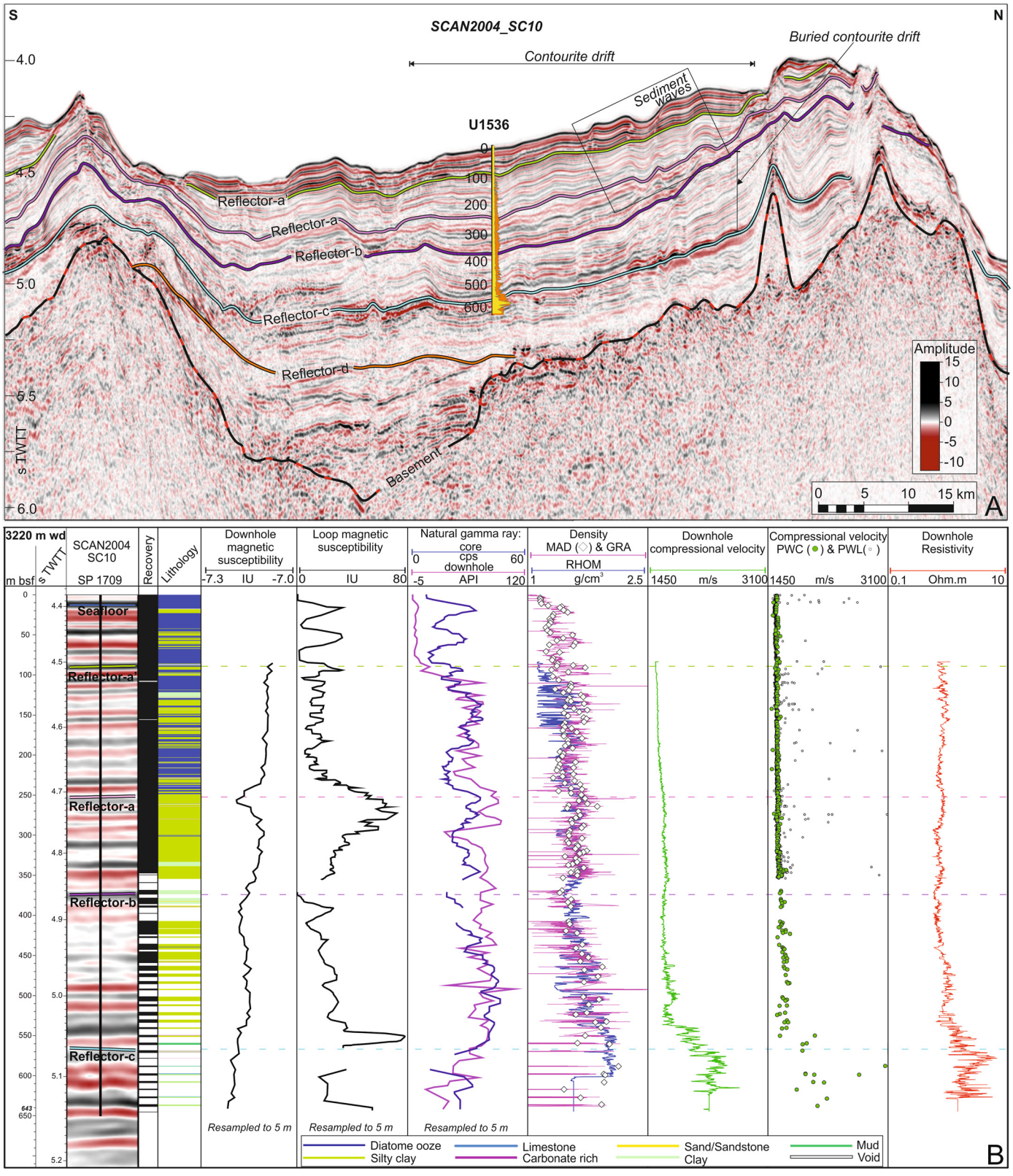

Fig. 2. Overview of Site U1536. A) Multichannel seismic profile SCAN2004_SC10. Seismic interpretation of the main stratigraphic discontinuities in Dove Basin and site location are included. For detailed seismic interpretation of the profile see Pérez et al. (2017). The overlain acoustic impedance logs are derived from: orange, downhole density and compressional velocity range between 1670-5270 Pa·s/m^3; and yellow, core-logged density and discrete compressional velocity measurements, range between 2770-7050 Pa·s/m^3. B) Physical properties of Site U1536 holes A and E, recorded during downhole and core logging. Note that magnetic susceptibility and natural gamma radiation logs have been resampled by running average to 5 m according to the interest of this work. The low recovery below 350 m results in scattered data in this area. Bsf, below seafloor; GRA, density from gamma-ray attenuation bulk densitometer; RHOM, downhole density; MAD, density from moisture and density samples; PWC, compressional velocity from P-wave caliper; PWL, compressional velocity from P-wave core-logger; SP, shot point; TWTT, two-way travel-time; wd, water depth. See Fig. 1 for location.

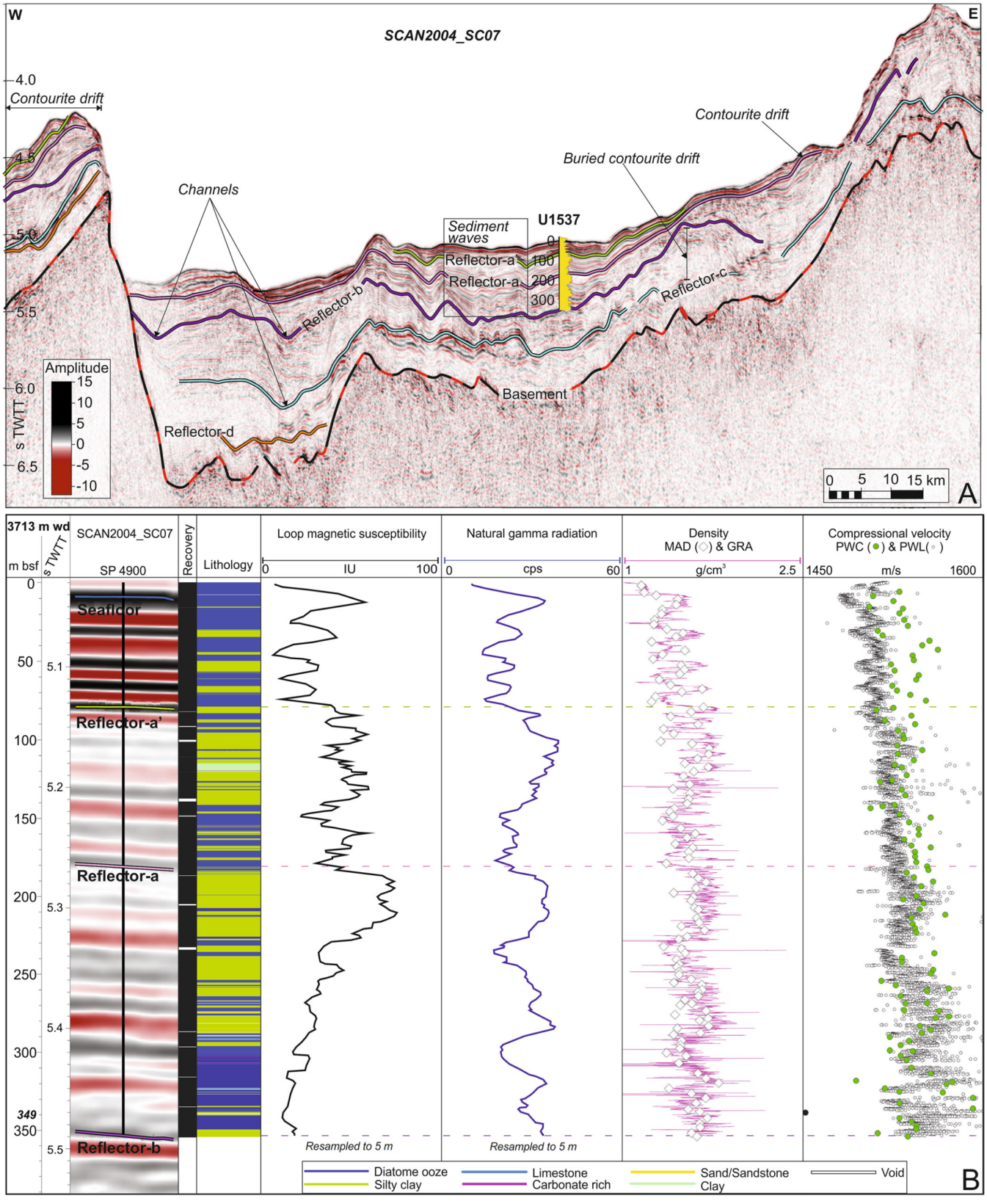

Fig. 3. Overview of Site U1537. A) Multi-channel seismic profile SCAN2004_SC07. Seismic interpretation of the main stratigraphic discontinuities in Dove Basin based on Pérez et al. (2017) and site location are included. The overlain acoustic impedance log in yellow is derived from core-logged density and discrete compressional velocity measurements, range between 1710-2800 Pa·s/m^3. B) Physical properties of Site U1537 hole D recorded during core logging. Note that magnetic susceptibility and natural gamma radiation logs have been resampled by running average to 5 m according to the interest of this work. Bsf, below seafloor; GRA, density from gamma-ray attenuation bulk densitometer; MAD, density from moisture and density samples; PWC, compressional velocity from P-wave caliper; PWL, compressional velocity from P-wave core-logger; SP, shot point; TWTT, two-way travel-time; wd, water depth. See Fig. 1 for location.

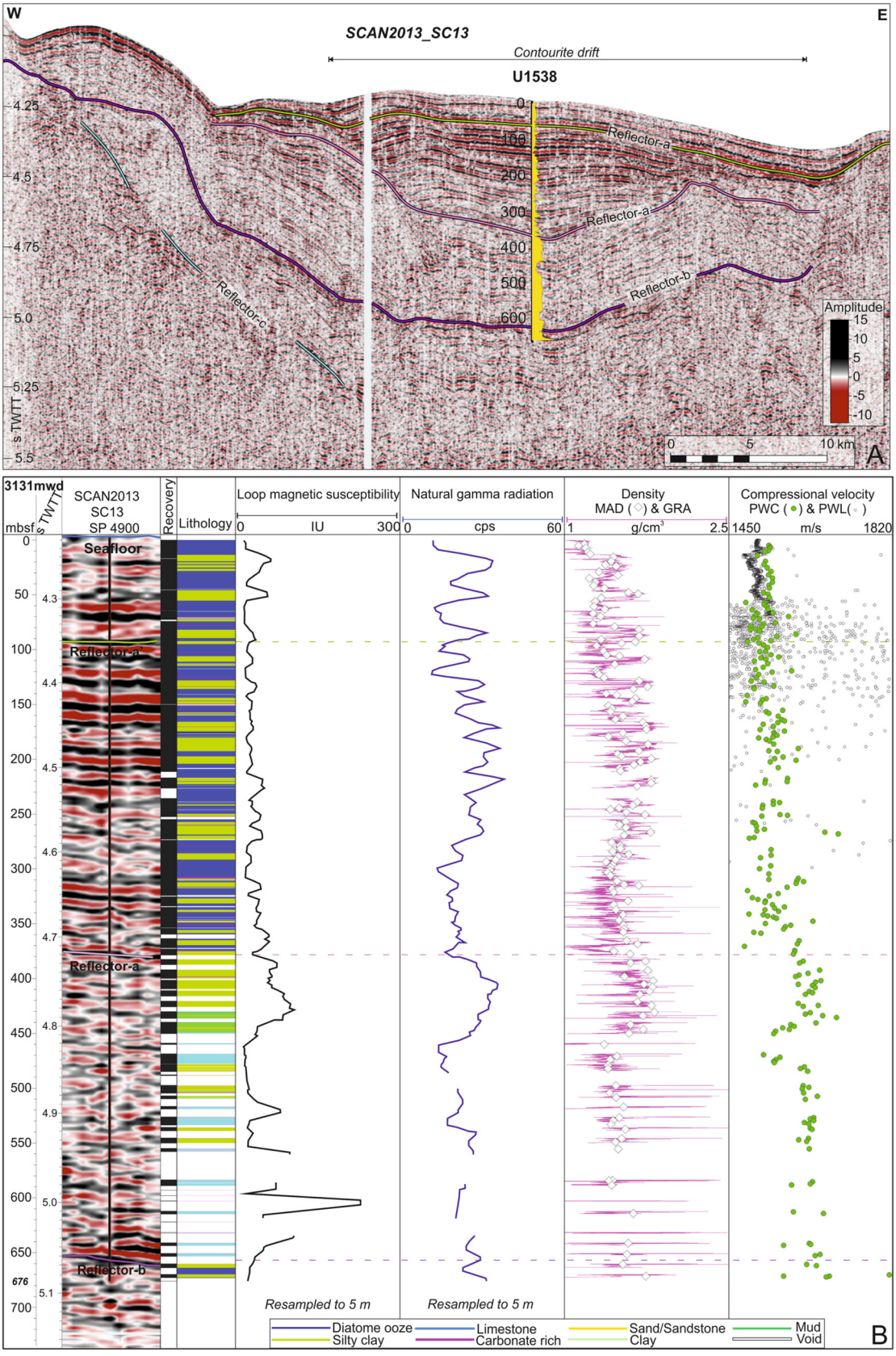

Fig. 4. Overview of the Site U1538. A) Single-channel seismic profile SCAN2013_SC13. Seismic interpretation of the main stratigraphic discontinuities in Pirie Basin and site location are included. The overlaid acoustic impedance log in yellow is derived from core-logged density and discrete compressional velocity measurements, range between 2850-3660 Pa·s/m^3. B) Physical properties of the Site U1538 hole A recorded during core logging. Note that magnetic susceptibility and natural gamma radiation logs have been resampled by running average to 5 m according to the interest of this work. The low recovery below 550 m results in scattered data in this area. Bsf, below seafloor; GRA, density from gamma-ray attenuation bulk densitometer; MAD, density from moisture and density samples; PWC, compressional velocity from P-wave caliper; PWL, compressional velocity from P-wave core-logger; SP, shot point; TWTT, two-way travel-time; wd, water depth. See Fig. 1 for location.

zonations were distinguished primarily based on first and last occurrences of diatoms, radiolarians and dinoflagellates on core catcher and shipboard samples (Weber et al., 2021). Biostratigraphic events and magnetic polarity intervals were interpreted relative to the geologic timescale following Gradstein et al. (2012). According to the IODP Expedition 382 chronostratigraphic constraints, an age range is given when the stratigraphic discontinuity is located between datums. An approximate interpolated age is obtained assuming linear sedimentation to the discontinuity depth. The displaced interpolated age takes into consideration the best dating of the three sites for each stratigraphic discontinuity (Table 1).

3. Age correlation of the regional discontinuities

Approximate ages were determined for the three drilled sites (U1536, U1537 and U1538; Fig. 1) based on biostratigraphic and paleomagnetic data (Fig. S1; Table S1), and are available in Weber et al. (2021). The oldest sediments recovered are from Site U1536 in Core U1536E-31R at ~80 m below Reflector-c (Fig. 2, 5) with an age younger than 15.97 Ma. Therefore, core-log-seismic correlation allows the characterisation with sediment physical properties and formation ages of the previously defined seismic-stratigraphic sequences of the upper sedimentary record of the Scotia Sea from late Miocene onwards (Fig. 2, 3, 4).

Reflector-c is well-characterised as a laterally continuous reflection within an interval of very high amplitude reflections in the seismic profiles (Fig. 2A, 3A; Fig. S2). The recovery in the stratigraphic interval containing this discontinuity is limited, which may be related to the presence of gravels and highly consolidated sediments and the rotary drilling procedure (Fig. 2B). However, downhole measurements show a change in the trend of the physical properties (Fig. 2B). While compressional velocity and resistivity values significantly increase downwards from ~549 mbsf, the major increase in the values is located at ~566 mbsf (5.07 s two-way travel-time TWTT) between Cores U1536E-25R and U1536E-27R, where we place Reflector-c. Sparse rock fragments in the lower cores of the site contain lithified mudstone and gravel-conglomerate-breccia, whereas mud and mudstone overly the discontinuity. Accordingly, the discontinuity represents a sharp upwards decrease in the formation resistivity and compressional velocity (PWC, >2000 m/s below to ~1700 m/s above). The density measured in the MAD samples decreases above the discontinuity (from 2.1 to 1.6 g/cm^3). The baseline of the core-log magnetic susceptibility increases from the sediments below Reflector-c towards the values observed above (16 to 33 IU). The same trend is followed by the total gamma radiation values of the downhole log, which increase from 28 API below to 60 API above the discontinuity (Fig. 2B), mainly related to the sharp increase in the potassium and thorium downhole logs (see HFK and HTHO logs in Weber et al., 2021). The diatoms recovered in Cores U1536E-26R to U1536E-30R are consistent with an age of about 8.4 Ma for the sediment directly overlying Reflector-c (Fig. 5; Table 1; Fig. S1; Table S1). The confident correlation of magnetic polarity zones to the Geomagnetic Polarity Time Scale ends a few meters above Reflector-c (Fig. 5; Table 1; Fig. S1). However, extrapolation of the depth-age trend based on geomagnetic reversal stratigraphy yields in an age of 8.6 Ma for sediments laying directly above Reflector-c, consistent with the biostratigraphy. The diatoms recovered from the sediments underlying Reflector-c in Core U1536E-31R suggest an age of 14.2 Ma (Fig. S1; Table S1). Therefore, Reflector-c could represent a prolonged period, or an event occurred anytime between 14.2 and 8.4 Ma and resulting in non-deposition or erosion at the location of Site U1536.

Reflector-b is found at the base of high amplitude and laterally continuous reflections in the seismic profiles (Fig. 2A, 3A, 4A; Fig. S2). It is set in silty clay sediments. However, recovery was low in the stratigraphic interval containing the reflection at both sites in Dove Basin (Fig. 2B). At Site U1536, Reflector-b is located at 375 mbsf (4.87 s TWTT) in Core U1536E-5R (Fig. 2B). The compressional velocity of the surrounding sediments is homogeneous with values of 1570 m/s in PWC and ~1660 m/s in downhole logged velocity. The average density of the section containing Reflector-b is ~1.4 g/cm^3, with very small differences (<0.2 g/cm^3) between the MAD, GRA and RHOM values. The stratigraphic location of Reflector-b coincides with a relative minimum in magnetic susceptibility (6 IU) and natural gamma radiation (~71API) values in the downhole logs (Fig. 2B). The biostratigraphic age constraint for Reflector-b is based on diatom and radiolarian species recovered in Cores U1536E-4R and U1536E-7R, suggesting an age range of 4.7-3.7 Ma (Fig. 5; Table 1). The paleomagnetic results agree with the younger age of the range (Fig. S1; Table S1). At Site U1537, Reflector-b is reached at 353 mbsf (5.49 s TWTT) in Core U1537D-48F, just at the bottom of the site (Fig. 3B). Diatoms from the deepest core point to an age range of 4.5-4.4 Ma for Reflector-b, and the paleomagnetic datums suggest an age >3.6 Ma (Fig. S1; Table S1). In Pirie Basin, Reflector-b is located at 660 mbsf (5.07 s TWTT) in Core U1538A-73X (Fig. 4B). The compressional velocity changes across Reflector-b from 1800 m/s below to 1550 m/s above. The density of the sediments below Reflector-b is higher (1.7 g/cm^3) with respect to the density of the sediments above it (1.5 g/cm^3). Velocity and density have an upward increase trend above Reflector-b marked by well-shaped changes correlating in both properties. High magnetic susceptibility (128 IU) and natural gamma radiation (38 cps) values coincide with the stratigraphic location of Reflector-b in Pirie Basin (Fig. 4B). The radiolarian recovered in Cores U1538A-73X to U1538A-75X point to an age between 4.6 and 3.5 Ma, whereas the identification of paleomagnetic reversals suggest a tentative older age range, 4.9-4.8 Ma (Fig. 5; Table 1; Fig. S1; Table S1).

Reflector-a constitutes a low amplitude reflection that is laterally continuous and defines the base of a section of highly laterally continuous reflections in the seismic profiles (Fig. 2A, 3A, 4A; Fig. S2). Reflector-a was drilled at all three sites, allowing a well constrained age determination (Fig. S1; Table S1). It is located in interbedded diatom ooze and silty clay in both Dove and Pirie basins (Fig. 2B, 3B, 4B). At Site U1536, Reflector-a is located at 254 mbsf (4.71 s TWTT) in Core U1536A-32F (Fig. 2B). Compressional velocity is homogeneous in the section, with values of ~1540 m/s and ~1600 m/s, in core and downhole measurements respectively. The measured density values are relatively high, with small discrepancies in the values among MAD (1.7 g/cm^3), GRA (1.8 g/cm^3) and RHOM (1.6 g/cm^3). The inferred position of Reflector-a coincides with an absolute maximum (>70 IU) on the core-log magnetic susceptibility curve and a relative maximum in natural gamma radiation values (86 API and 39 cps on downhole and core logs respectively). The recovered microfossils between Cores U1536A-30F and U1536A-32F suggest an age of 1.8-1.4 Ma for Reflector-a, whereas paleomagnetic data suggest 1.7 Ma (Fig. 5; Table 1; Fig. S1; Table S1). At Site U1537 Reflector-a is located at 180 mbsf (5.26 s TWTT) in Core U1537D-20F (Fig. 3B). It coincides with stratigraphic-upwards transitions from higher to lower values of velocity (1550-1530 m/s), density (1.6-1.4 g/cm^3), magnetic susceptibility (91-22 IU) and natural gamma radiation (>25-<9 cps). Diatom and radiolarian datums suggest an age range of 1.7-1.5 Ma in Cores U1537A-20H to U1537A-22H, and the paleomagnetic data suggest 1.5 Ma (Fig. 5; Table 1; Fig. S1; Table S1). In Pirie Basin, Reflector-a is located at 370 mbsf (4.72 s TWTT) in Core U1538A-43X, denoting a change in the seismic pattern towards more stratified and continuous reflections above it (Fig. 4). The discontinuity coincides with a sharp decrease in compressional velocity values from >1600 m/s below to 1550 m/s above it. A rel-

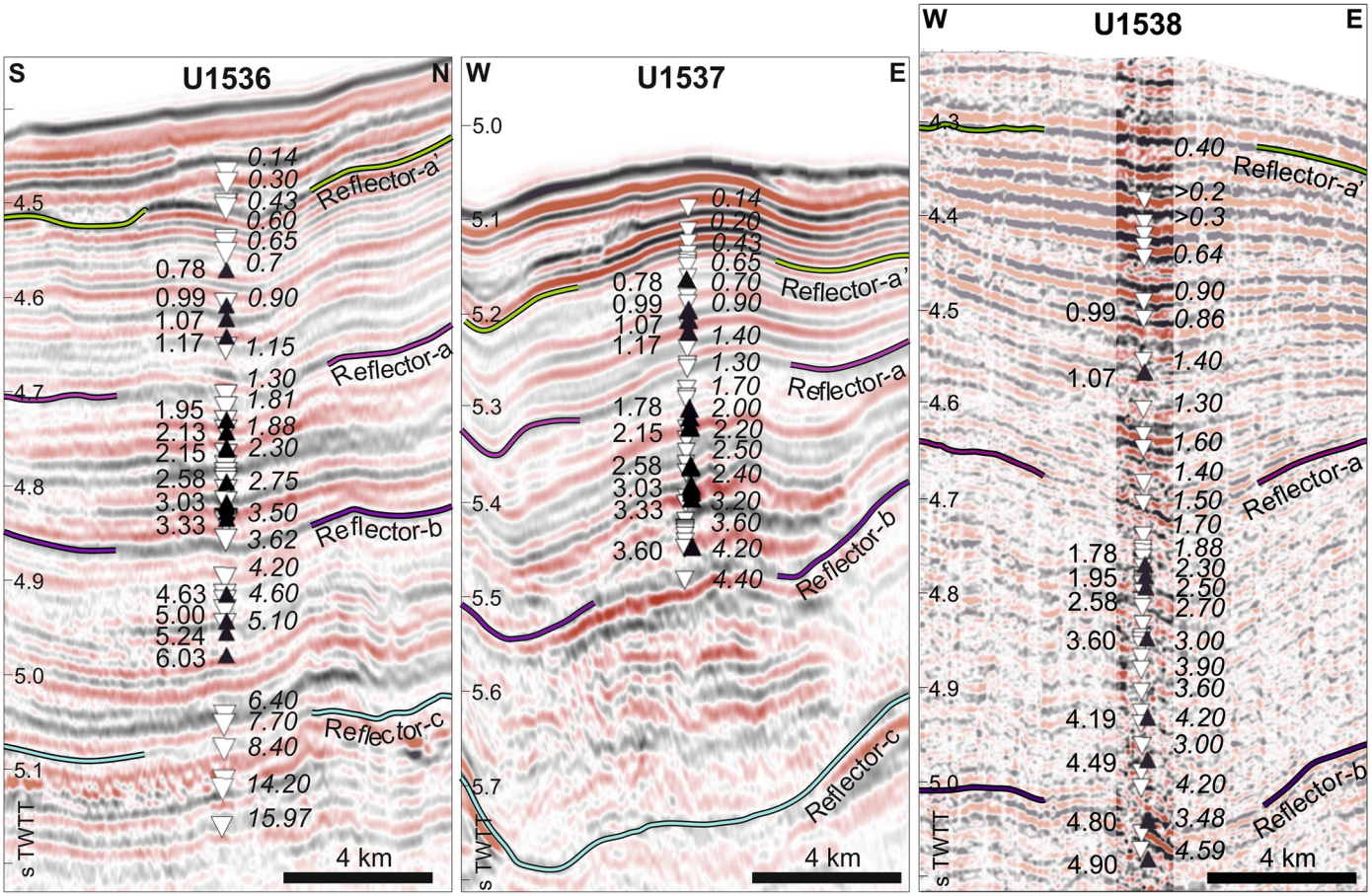

Fig. 5. Age constrains of the sites over seismic background. White and black triangles represent the ties of the biostratigraphic and paleomagnetic ages, respectively. The major stratigraphic discontinuities are marked. TWTT, two-way travel-time.

ative minimum in density (MAD 1.4 g/cm^3) correlates with the discontinuity, whereas the sediments below it present generally higher density (1.7 g/cm^3) than above it (1.5 g/cm^3). Maximum magnetic susceptibility (79 IU) and minimum natural gamma radiation (>10 cps) values coincide with Reflector-a, whereas the baselines of both physical properties present higher values in the sediments below with respect to the sediments above Reflector-a (Fig. 4B). The diatoms at Site U1538 suggest an age of 1.7-1.5 Ma for Reflector-a, close to the age of 1.6 Ma suggested by paleomagnetic datums (Fig. 5; Table 1; Fig. S1; Table S1).

Reflector-a' represents the uppermost stratigraphic discontinuity drilled in the three sites of the Scotia Sea during IODP Expedition 382. In the seismic record, it is characterized by a high amplitude and laterally continuous reflection at the base of a stratified pattern (Fig. 2A, 3A, 4A). Reflector-a' represents the contact between diatom ooze and silty clay interbedded layers. In Dove Basin, Reflector-a' is located at 90 mbsf (4.51 s TWTT) between Cores U1536A-10H and U1536A-11H (Fig. 2B). The overlying downhole measurements are affected by the pipe emplacement and are not considered in the description here. The compressional velocity is relatively constant within the section (~1500 m/s). Reflector-a' coincides with a relative maximum in density (MAD) and magnetic susceptibility values of 1.7 g/cm^3 and ~40 IU, respectively, and a sharp upwards decrease in natural gamma radiation values from >35 cps below it to <10 cps above it (Fig. 2B). The diatom datums in Cores U1536A-10H to U1536A-13H suggest an age of 0.6-0.4 Ma for Reflector-a' (Fig. 6; Table 1; Fig. S1; Table S1). At Site U1537, Reflector-a' is reached at 80 mbsf (5.13 s TWTT), at the bottom of Core U1537D-9H (Fig. 3B). The compressional velocity values are similar to the neighbouring site (~1540 m/s). However, low density sediments (MAD 1.3 g/cm^3) form Reflector-a'. Low magnetic susceptibility (~6 IU) and natural gamma radiation (11 cps) values have been measured at Reflector-a' (Fig. 3B). The radiolarians of Core U1537D-9H suggest an age of 0.6 Ma (Fig. 5). In Pirie Basin, Reflector-a' is reached at 90 mbsf (4.35 s TWTT) between Cores U1538A-9H and U1538A-10H (Fig. 4B). The discrete core measurements show highly variable compressional velocity values in the surroundings of Reflector-a' (1490-1540 m/s). Reflector-a' represents a sharp upwards decrease in density (MAD 1.8-1.3 g/cm^3) and natural gamma radiation (40-8 cps) values. The core-log magnetic susceptibility at the discontinuity is 21 IU (Fig. 4B). The biostratigraphy suggests an age under 0.4 Ma for Reflector-a' in U1538 (Fig. 5; Table 1; Fig. S1; Table S1).

4. Local sedimentation rates

Sedimentation rates between the major stratigraphic discontinuities have been calculated based on the age model obtained during IODP Expedition 382 (Weber et al., 2021). The sedimentation rate in Dove Basin during the late Miocene (8.4-4.5/3.7 Ma), i.e. between Reflector-c and Reflector-b, was 4.1-4.9 cm/kyr (3.7-6.4 cm/kyr considering maximum and minimum ages of the discontinuities at Site U1536; Fig. 6; Table 1; Fig. S1). Pliocene-early Pleistocene (4.5/3.7-1.7 Ma) sedimentation occurred between Reflector-b and Reflector-a at rates between 4.6-6.1 and 5.2-9.6 cm/kyr in Dove Basin at Sites U1536 and U1537 respectively, and 10.4-14.5 cm/kyr in Pirie Basin at Site U1538 (Fig. 6). Sediments accumulated between Reflector-a and Reflector-a' during the early Pleistocene (1.7-0.4 Ma) at sedimentation rates between 12.6 and 7.7 cm/kyr in Dove Basin at Sites U1536 and U1537 respectively,

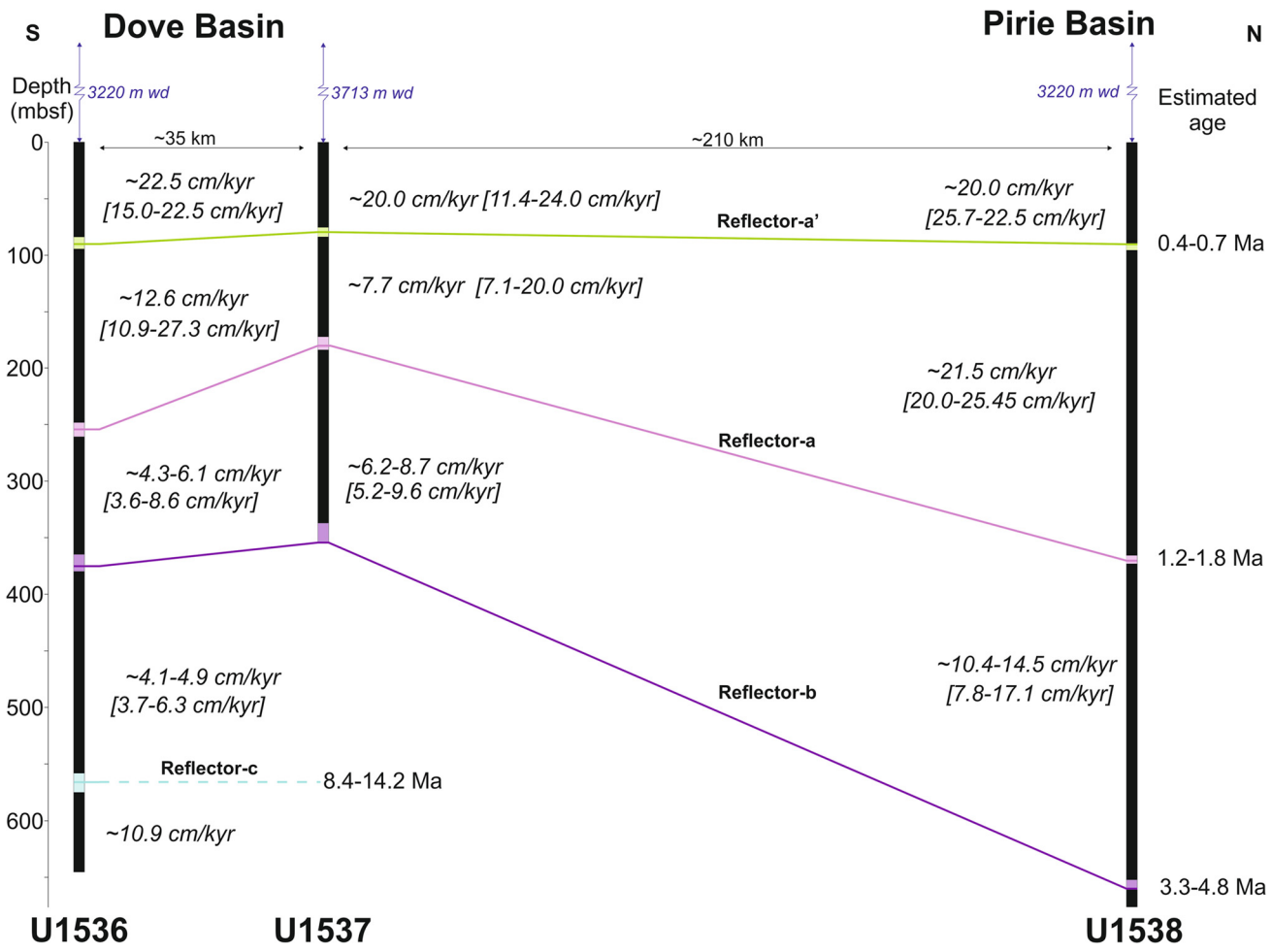

Fig. 6. Fence diagram with the estimated sedimentation rates for Sites U1536, U1537 and U1538 based on the age models from IODP Expedition 382 (Weber et al., 2021). The colour shaded areas on the sites correspond to the depth range of the stratigraphic discontinuities. The ranges of the sedimentation rate correspond to maximum and minimum ages considerations. bsf, below sea floor; wd, water depth.

and 21.5 cm/kyr in Pirie Basin at Site U1538. The youngest sedimentary record (after 0.4 Ma), above Reflector-a', deposited from the Mid-Pleistocene to recent has the highest sedimentation rates at all three sites reaching over 20.0 cm/kyr in both Dove and Pirie basins (Fig. 6).

The local sedimentation rates on the drilled sites are generally higher in Pirie Basin than in Dove Basin, and generally increase upwards in the stratigraphic column (Fig. 6). Partial downwards decrease in the calculated sedimentation rates is expected from the compaction effect and porosity reduction. However, for near-equivalent depth intervals, from early Pleistocene to present the sedimentation rates in the southern part of Dove Basin (U1536) were higher than in its northern part (U1537), whereas they followed an opposite trend prior to the early Pleistocene (Fig. 6). Previously published studies of sediment distribution in the Scotia Sea (Pérez et al., 2014, 2017, 2019) suggest that none of the IODP Expedition 382 sites are located over local or regional depocentres where the highest sedimentation rates are expected.

5. Updated age correlation

Several previous studies investigated the seismic-stratigraphy of the Scotia Sea (e.g., Maldonado et al., 2006, 2014; Martos et al., 2013, Pérez et al., 2014, 2017, 2019). However, the lack of deep drilling in the region prevented establishment of an accurate age model for the main stratigraphic discontinuities as defined by these studies. The ages of the stratigraphic discontinuities were commonly estimated assuming continuous sedimentation rates, extrapolated from Jane Basin (Fig. 1), over the underlying igneous crust, which age was based on models of spreading magnetic anomalies (Maldonado et al., 2006). Ocean Drilling Program (ODP) Site 697 drilled during Leg 113 is located in the centre of Jane Basin (Gersonde et al., 1990), to the south of the Scotia Sea (Fig. 1), but it provided the only available chronostratigraphic information prior to IODP Expedition 382. Major stratigraphic changes in the Jane Basin seismic record where dated according to the ODP Site 697, and then extrapolated to the Scotia Sea by means of seismic facies comparison (e.g., Maldonado et al., 2006). Table 1 shows a comprehensive view of the ages of the major discontinuities as obtained from IODP Expedition 382 (Table S1) and previously estimated ages. Overall, the ages of the main stratigraphic discontinuities obtained from IODP Expedition 382 are between 2.7 and 2.0 Myr younger than previously estimated from igneous crust models and far field sedimentation rates. Reflector-c previously estimated formation age was 12.6 Ma (Maldonado et al., 2006), however, drilling confirms it formed sometime between 14.2 and 8.4 Ma (Table 1).

6. Global implications

Taking into consideration different tectonic reconstructions of the opening of the Drake Passage and the formation of the Scotia Sea (e.g., Eagles et al., 2006; Galindo-Zaldívar et al., 2006, 2014; Dalziel et al., 2013; Eagles and Jokat, 2014; Maldonado et al.,

Table 1
Ages of the main regional discontinuities in Ma as resolved in the three sites during IODP Expedition 382 (Weber et al., 2021) and compared with the previous ages estimated by Maldonado et al. (2006) and age of the Reflector-a' estimated in Pérez et al. (2017). The interpolated age is calculated from the closest and more accurate age values by linear interpolation to the stratigraphic discontinuity depth. Note that the interpolated age of Reflector-c corresponds to the time interval missing at Site U1536 and two possible interpolated ages are given for Reflector-b. The biostratigraphic and paleomagnetic datums that support these ages are included in the supplementary Table S1.

Stratigraphic discontinuity	U1536		U1537		U1538		Resolved in this work		Previous ages (Maldonado et al., 2006) & (Pérez et al., 2017) (Ma)
	Biostrat. (Ma)	Pmag. (Ma)	Biostrat. (Ma)	Pmag. (Ma)	Biostrat. (Ma)	Pmag. (Ma)	Interval (Ma)	Interpolated (Ma)	
Reflector-a'	0.4-0.6	-	0.4-0.7	-	~0.4	-	0.4-0.7	**0.4**	2.6
Reflector-a	1.3-1.8	1.2-1.9	1.3-1.7	1.2-1.8	1.5-1.7	1.1-1.8	1.2-1.8	**1.7**	3.8
Reflector-b	3.6-4.2	3.3-4.6	4.4-4.5	>3.6	3.5-4.6	4.5-4.8	3.3-4.8	**4.5/3.7**	6.4
Reflector-c	~8.4	*~8.6*	-	-	-	-	>8.4	***>8.4 & <14.2***	12.6

2014), the sediments recovered within the three sites of IODP Expedition 382 were not deposited until the southern Scotia Sea sedimentary basins, including Dove and Pirie Basin (Fig. 1), were fully opened (Pérez et al., 2019). The core-log-seismic correlation presented here suggests three major phases in the tectonic, oceanographic and climatic evolution of the region from the middle-late Miocene to the present-day.

6.1. Phase 1: late Miocene sedimentary switch

The seismic record of the southern Scotia Sea reveals a major reorganization of the regional sedimentary stacking pattern leading to the formation of Reflector-c. According to the drilling record, Reflector-c represents either a period of non-deposition, a highly condensed sequence, or possibly even the result of sediment winnowing or erosion in Dove Basin at some time between 14.2 and 8.4 Ma (Fig. 5; Table 1).

It has been suggested that the sedimentary change that created Reflector-c was related to a major change in the regional oceanic circulation pattern (e.g., Maldonado et al., 2006). On a regional scale, the seismic stratigraphy below discontinuity Reflector-c suggests minimal influence of deep-water flows, whereas sedimentation overlying Reflector-c appears to be controlled by the near-bottom currents (e.g., Maldonado et al., 2006; Pérez et al., 2019). This inference is mainly based on the configuration of the seismic reflections observed in the dataset of the southern Scotia Sea, where most of the sediment waves and contourite drifts have been identified above Reflector-c. The evidence of deep-water flow impact identified on the seismic record below Reflector-c is limited to a few buried drifts that suggest an eastward flow emplaced in the Scotia Sea, related to the CDW circulation (e.g., Pérez et al., 2014, 2017, 2019). The diversion of the near-bottom water mass during the sedimentation above Reflector-c generated northwestward migration of depocentres and formed well-developed current-related features in all of the southern Scotia Sea basins related to the WSDW flow (e.g., Maldonado et al., 2006, 2014; Martos et al., 2013; Pérez et al., 2014, 2017). The northward inflow of WSDW into the Scotia Sea constitutes the major change in the oceanic circulation pattern at a regional scale since the Drake Passage formation (e.g., Maldonado et al., 2006). The onset of this new oceanic circulation pattern in the Scotia Sea is represented by the Reflector-c and occurred between 14.2 and 8.4 Ma.

Site U1536, located on the abyssal plain of Dove Basin, is in the path of WSDW inflow through the deepest oceanic gateway in the South Scotia Ridge (Fig. 1), the Orkney Passage (ca. 3800 m water depth) (Pérez et al., 2017). The increase in the magnetic susceptibility of Site U1536 sediments deposited above Reflector-c could be caused by an increase influx of terrigenous material to the Scotia Sea via WSDW inflow (Fig. 2B). Equally, the increase in the natural gamma radiation of these sediments and in their clay content above Reflector-c in Dove Basin (Fig. 2B), could be the product of mobilisation of sediment from the Antarctic continental shelves (e.g., Diekmann et al., 2004) after 8.4 Ma, as a result of a broad expansion of the Antarctic ice sheets. The time interval associated with Reflector-c (14.2-8.4 Ma), coincides with a positive benthic $\delta^{18}O$ shift (Fig. 7) and near-modern values in sea-surface temperature (Herbert et al., 2016) interpreted to reflect a global glaciation event during late Miocene – early Pliocene (Table 2). Consequently, with the late Miocene ice advance, global eustatic sea level was relatively low (Miller et al., 2005). Low obliquity and high eccentricity orbital parameters during late Miocene favoured the onset of perennial sea ice (Levy et al., 2019), as well as the northward expansion of the West Antarctic and Antarctic Peninsula ice sheets (e.g., Anderson et al., 2011). As a result of the ice sheets expansion, the formation of WSDW may have increased, establishing its outflow towards the Scotia Sea. Consequently, the ACC and the polar fronts migrated northward (Fig. 7) (e.g., Maldonado et al., 2006; Pérez et al., 2019) further promoted by the uplift of the Shackleton Fracture Zone and the regional change towards a compressive tectonic regime that could modify the gateways between Weddell and Scotia seas (Livermore et al., 2004; Hernández-Molina et al., 2006; Bohoyo et al., 2007; Martos et al., 2013).

6.2. Phase 2: Pliocene – early Pleistocene oceanic circulation enhancement

Reflector-b represents a regional stratigraphic change previously related to strong incursions of the WSDW into the Scotia Sea and the SPDW flowing through the Drake Passage (Martos et al., 2013; Pérez et al., 2017). According to the IODP Expedition 382 age models (Weber et al., 2021), Reflector-b formed between 4.8 and 3.3 Ma. The accuracy of the discontinuity identification allows for two possible regional interpolated ages of either ~4.5 Ma or ~3.7 Ma (Fig. 5; Table 1). Reflector-b corresponds to relative minimum values in magnetic susceptibility in the sediments of Dove and Pirie basins (Fig. 2B, 3B, 4B). If it formed by ~4.5 Ma, Reflector-b could constitute the onset of the global trend toward warm climatic conditions of early Pliocene (e.g., Pollard and DeConto, 2009). The Antarctic ice sheets largely retreated leading to high global sea level (Fig. 7) and enhancement of Southern Ocean deep-water circulation (e.g., Kwiek and Ravelo, 1999). Strengthened deep flows would favour the widespread formation of current-related features in the Scotia Sea such as those observed in the sedimentary record above Reflector-b (Fig. 2A, 3A, 4A), while locally creating erosive signatures (Pérez et al., 2017, 2019). The Pliocene global warmth predated the cold trend initiated at ~3.7 Ma (e.g. Pollard and DeConto, 2009), reflected in high magnetic susceptibility and natural gamma radiation baselines below Reflector-a (Fig. 2B, 3B, 4B). These overall high values in the physical properties potentially track a progressive rise in the relative abundance of terrigenous material derived from the enhanced outflow of WSDW towards the Scotia Sea once the Antarctic ice sheets extended over the continental shelf (Fig. 7; Table 2) and the eustatic sea level dropped from ~10 above to ~50 m below present-day level (Rohling et al., 2014). The late Pliocene WSDW/LCDW expansion through the Atlantic Ocean led once again to the northward migration of oceanic fronts (e.g., Sijp and England, 2004; McKay et al., 2012).

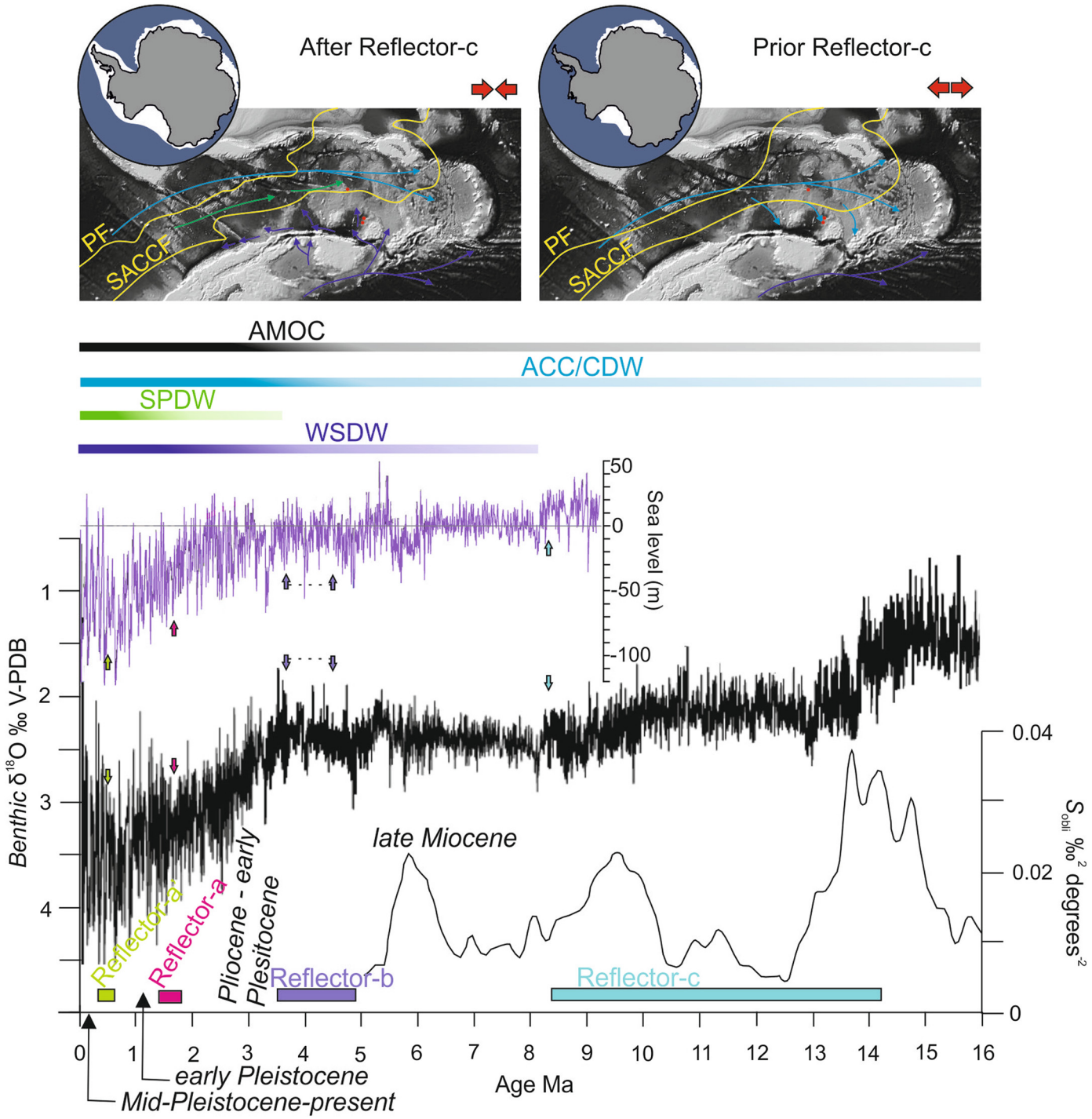

Fig. 7. Correlation of the regional stratigraphic discontinuities of the Scotia Sea with the megasplice of benthic $\delta^{18}O$ global records as published by De Vleeschouwer et al. (2017). Sea level curve is from Miller et al. (2005). The colour arrows and bars represent the discussed stratigraphic discontinuities, note the alternate age for Reflector-b. Obliquity curve and configurations of the Antarctic ice sheets as published in Levy et al. (2019). The ice sheet configurations represent none to occasional marine-based ice sheets over the Antarctic continental shelf on the right, prior to Reflector-c; and perennial-marine based ice sheets on the left, after Reflector-c based on previous regional interpretations (e.g. Levy et al., 2019). The red arrows represent the overall regional tectonic extension (right) or compression (left) during these time periods based on e.g., Bohoyo et al. (2007). Bottom water flow across the Scotia Sea prior and after Reflector-c formation represented by the present-day bathymetry, note the bathymetry of the Shackleton Fracture Zone is considered only after the onset of its uplift around the time of Reflector-c formation. Colours as water masses below. The colour gradation of the bars represents the relative enhancement of the flows. AMOC, Atlantic Meridional Overturning Circulation; ACC, Antarctic Circumpolar Current; CDW, Circumpolar Deep Water; SPDW, South Pacific Deep Water; WSDW, Weddell Sea Deep Water. The yellow lines represent the estimated location of the Polar Front (PF) and South ACC Front (SACCF). The red dots point to the location of Sites U1536, U1537 and U1538.

Given the lack of tighter constrains, the uncertainty of Reflector-b age may alternatively suggest correlation of the discontinuity with the cooling trend initiated at ~3.7 Ma (Fig. 7), hence, broadly coinciding with the inferred maximum AMOC vigour after the Central American Seaway constriction reached a hypothesised critical threshold at ~4 Ma (Karas et al., 2017). A subsequent decline in AMOC from ~3.8 Ma has been proposed to have helped precondition the high northern latitudes for glaciation through attendant cooling and sea-ice formation (e.g., Karas et al., 2017). A heightened AMOC activity would have transferred more North Atlantic

Table 2
Summary of the environmental conditions at the time frames defined by the discussed stratigraphic discontinuities, see text for details. ACC, Antarctic Circumpolar Current; AMOC, Atlantic Meridional Overturning Circulation; LCDW, Lower Circumpolar Deep Water; SPDW, South Pacific Depth Water; WSDW, Weddell Sea Deep Water.

Oceanography	Climate & Sea-level	Tectonics	Scotia Sea Stratigraphy
• Energetic ACC • High production and outflow of WSDW • Dynamic AMOC	• West Antarctica and Greenland ice sheets collapse • Large amplitude of glacial-interglacial oscillation • Global sea-level above that of today	• Quiet tectonic context	• High regional sedimentation rates • Fast growth of the contourite drifts
Reflector-a': 0.6-0.4 Ma			
• WSDW flows through the Scotia Sea • Enhanced SPDW flow due to enhanced Pacific Overturning Circulation	• Antarctic, sub-Arctic, Mediteranean cooling • Pacific Cold Tonge • Intensification of Eurasian and Antarctic glaciations • Sharp drop in sea-level	• Quiet tectonic context	• Northeastward migration of regional depocentres • Fast growth of the contourite drifts
Reflector-a: 1.8-1.4 Ma			
• WSDW/LCDW expansion through the Atlantic Ocean • Northward migration of oceanic fronts • SPDW flow through the Drake Passage • Decline in AMOC	• High eustatic sea level followed by drop below present-day level • Early Pliocene warmth followed by high latitudes cooling and sea-ice formation	• Enhanced uplift of the Shackleton Fracture Zone • Continued uplift of the Transantarctic Mountains	• Increasing number of current-related features • Onset of growth of large contourite drifts in the northern part of Pirie Basin
Reflector-b: 4.9-3.5 Ma			
• Increase in WSDW formation and outflow towards the Scotia Sea • Northwards migration of the ACC fronts • Expansion of the Antarctic Ice Sheet	• Expansion of the Antarctic Ice Sheet (West Antarctic and Antarctic Peninsula ice sheets) • Relatively low global eustatic sea-level	• Uplift of the Shackleton Fracture Zone	• Northwestward migration of depocentres • Current-related features in the southern Scotia Sea basins related to northwestward flow
Reflector-c: 14.2-8.4 Ma			
• ACC flow across Scotia Sea	• Mid-Miocene Climatic Optimum	• Very active tectonic context	• Sparse buried drifts related to eastward flow

Deep Water to the Southern Ocean likely contributing to enhanced formation of WSDW and northward throughflow of AABW in the Scotia Sea (McKay et al., 2012).

Pirie Basin is protected from the influence of the WSDW outflow and instead more exposed to influence of the eastward flows due to its morphological configuration. Site U1538 is located today just to the north of the Southern ACC Front, and therefore under the influence of SPDW (Naveira-Garabato et al., 2002). Reflector-b in the northern part of Pirie Basin forms the base of large contourite drifts resulting from the influence of an eastward current that delivered the clay observed in the lithological record (Fig. 4A, 7). The formation of Reflector-b could be related to the SPDW flowing through the Drake Passage north of the Southern ACC Front. The historic variability of this water mass has been linked to the Central American Seaway closure (Kwiek and Ravelo, 1999). However, the time of closure of the Central American Seaway is still highly debated and ranges from Miocene (e.g., Montes et al., 2015) to Mid-Pliocene (e.g., O'Dea et al., 2016). The continued uplift of the Transantarctic Mountains (van Wijk et al., 2008) and the enhanced uplift of the Shackleton Fracture Zone (Livermore et al., 2004; Martos et al., 2013) constrained the oceanic flows through the Drake Passage. Thus, the deep eastward inflow to the Scotia Sea was limited to the northernmost part of the gateway (Fig. 7). This tectonic constraint could explain the development of contourite drifts in Pirie Basin from the Pliocene flow of SPDW through the Drake Passage.

6.3. Phase 3: mid-Pleistocene oceanic circulation pattern adjustment

Reflector-a has been traditionally interpreted as the onset of the modern oceanic circulation pattern in the Scotia Sea with a previously estimated age of 3.8 Ma (Pérez et al., 2017). According to the age models obtained during IODP Expedition 382 (Weber et al., 2021), Reflector-a was regionally formed between 1.8 and 1.4 Ma (~1.7 Ma; Fig. 5; Table 1). Values of magnetic susceptibility and natural gamma radiation generally decrease above Reflector-a at all three Scotia Sea sites (Fig. 2B, 3B, 4B), which may record sedimentation controlled by the strong oceanic flows instead of sediment transport from the Antarctic continental shelf. Abundant diatom ooze sedimentation above Reflector-a agrees with the decrease in sediment input from the Antarctic continental shelf (Fig. 2B, 3B, 4B). The active bottom flows generated a northeastward migration of the regional depocentres (Pérez et al., 2019). WSDW flows through the Scotia Sea, which have been under tectonic quiescence after the end of the compression in the Andean Cordillera (Torres-Carbonell et al., 2014) and the last increase in the East Scotia Ridge activity (Table 2) (Larter et al., 2003) before Reflector-a formation. In Pirie Basin, a marked change in the seismic facies of the sedimentary record of the contourite drifts occurs above Reflector-a together with a sharp increase in the sedimentation rate at Site U1538 (Fig. 4A, 6) owing to fast growth of the contourite drifts. The fast growth of these drifts from the Mid-Pleistocene to the present may be related to enhanced SPDW flow driven by the enhanced Pacific Overturning Circulation (e.g., Kwiek and Ravelo, 1999).

The high sediment input would have been provided through the ice sheet advance over the Antarctic continental shelf since Reflector-a was formed broadly around the same time in the Scotia Sea than the markedly cold trend in sub-Antarctic (Martínez-García et al., 2010), (sub)Arctic (e.g., Martínez-García et al., 2010) and Mediterranean (Herbert et al., 2015) regions and the development of the modern equatorial Pacific Cold Tongue (~1.6-1.8 Ma; Martínez-García et al., 2010). Evidence also exists that Eurasian (e.g., Herbert et al., 2015) and Antarctic (Pollard and DeConto, 2009) glaciations intensified at this time. Sea level experienced a sharp drop predating an increase in the benthic $\delta^{18}O$ (Rohling et al., 2014). Therefore, the development of Reflector-a at ~1.7 Ma most likely reflects the regional Southern Hemisphere expression of major global climatic changes.

The oceanographic control over the sedimentation in the Scotia Sea is particularly remarkable above the uppermost stratigraphic discontinuity highlighted in Dove and Pirie basins' record, Reflector-a' (Pérez et al., 2017). Reflector-a' was previously related to the onset of the Northern Hemisphere glaciation. However, IODP Expedition 382 age models reveal that Reflector-a' was formed between 0.6 and 0.4 Ma (Fig. 5; Table 1). Therefore, the last major change in the oceanic circulation pattern of the Scotia Sea falls within the time interval of Marine Isotope Stage (MIS) 11, ~0.4 Ma (Fig. 7). Global sea-level during this interglacial was between 6 and 13 m above that of today (Raymo and Mitrovica, 2012; Rohling et al., 2014). This high-stand is typically related to the West Antarctica and Greenland ice sheets collapse with limited contribution from East Antarctica (Table 2) (e.g., Raymo and Mitrovica, 2012; Hatfield et al., 2016; Wilson et al., 2018). The change in the physical properties of the Scotia Sea records related to Reflector-a' is likely associated with the large amplitude of the glacial-interglacial oscillations occurring after the Mid-Brunhes Transition (Barth et al., 2018). Low values of magnetic susceptibility in the Scotia Sea records linked to lower siliciclastic/bioclastic input rates (Fig. 2B, 3B, 4B) after MIS11 may reflect limited extension of the Antarctic ice sheets. However, an active regional oceanic circulation pattern controlling the sedimentation may have been maintained through energetic ACC and high production of WSDW. A generally high WSDW outflow through Scotia Sea after Reflector-a' would be consistent with the high sedimentation rates (Table 2), and only supported with relative diminution of AABW volume limited to extreme interglacials (Barth et al., 2018). In turn, a recent study reported lack of WSDW export into the Atlantic sector of the Southern Ocean during the last two glacial maxima (Huang et al., 2020). The ACC and WSDW flows would have been maintained by dynamic AMOC (Fig. 7). During MIS11, the AMOC was apparently energetic due to a distinct origin and rate of meltwater production (Doherty and Thibodeau, 2018).

7. Conclusions

Four main stratigraphic discontinuities in the sedimentary record of the Scotia Sea have been identified in both the seismic records and the physical properties measured by wireline downhole and core-log in three drilled sites during IODP Expedition 382. The age models and core-log-seismic correlation developed during the expedition revealed that the main discontinuities are much younger than previously proposed, correlating with major changes in the global environmental conditions.

The large-scale variability of the Antarctic ice sheets appears to be closely linked to the increasing formation of Weddell Sea Deep Water and the broad dynamics of the Antarctic Circumpolar Current. The interplay of regional tectonic and oceanography with global climatic trends has resulted in a progressive enhancement of near-bottom circulation in the Scotia Sea from the late Miocene.

The main change in the oceanic circulation pattern of the Drake Passage and Scotia Sea since its formation occurred between 14.2 and 8.4 Ma as consequence of the inflow of Antarctic Bottom Water from the Weddell Sea. This change was previously dated as 12.6 Ma, however, the broader age range between the sediments below and above the Reflector-c is either related to long tectonic processes accompanying the opening of the Southern Scotia Ridge deep gateways, or erosive/non-depositional intrusion of the Weddell Sea Deep Water before 8.4 Ma. According to the newly determined ages, the change was established by the time of the expansion of the West Antarctic and Antarctic Peninsula ice sheets during late Miocene.

After the late Miocene, the oceanic circulation pattern of the Scotia Sea experienced marked evolutionary steps at ~4.5/3.7 Ma and ~1.7 Ma. Previously, these two stratigraphic changes were estimated to occur at 6.4 Ma and 3.8 Ma. The formation of Reflector-b could have occurred at ~4.5 Ma during global warm conditions and active Southern Ocean oceanic circulation; or at ~3.7 Ma in relation to strong outflow of the Weddell Sea Deep Water through the Scotia Sea due to Antarctic ice sheets expansion. In both scenarios, energetic Antarctic Circumpolar Current and South Pacific Deep Water flows are inferred from the records. At ~1.7 Ma, Reflector-a resulted from the onset of the modern oceanic circulation pattern in the Scotia Sea, coinciding with the Northern Hemisphere trend towards a cold climate and the global intensification of glacial conditions. Lastly, very active oceanic circulation pattern in the Scotia Sea during the formation of Reflector-a' at ~0.4 Ma could relate to a dynamic Atlantic Meridional Overturning Circulation during Marine Isotope Stage (MIS) 11.

Strong differences in the seismic record between the southern and central Scotia Sea after Mid-Pliocene are mainly related to the flow of South Pacific Deep Water along the central Scotia Sea while the southern Scotia Sea has been under the influence of Weddell Sea Deep Water from late Miocene onwards. As a result, Dove and Pirie basins have evolved under markedly different oceanographic conditions.

CRediT authorship contribution statement

All authors contributed to the collection and interpretation of datasets presented in this paper and manuscript discussions. LFP led the data analyses and integration, and manuscript writing. YMM and MG actively contributed to the core-log-seismic correlation. MEW and MER were co-chief scientists of IODP Expedition 382, TW was staff scientist in the expedition. They contributed to project design and manuscript writing. FB contributed to the seismic data acquisition and interpretation. This work was conducted as a key output of the IODP Expedition 382 Scientific Party, and the scientific party is acknowledged for their shipboard work. LFP wrote the Marie Curie Fellowship proposal and NERC projects that funded this work.

Declaration of competing interest

The authors declare that they have no known competing financial interests or personal relationships that could have appeared to influence the work reported in this paper.

Acknowledgements

The first author and this work have received funding from the European Union's Horizon 2020 research and innovation programme under the Marie Skłodowska-Curie grant agreement No. 792773 Global Fellowship H2020-MSCA-IF-GF-2017 WAMSISE and the Natural Environment Research Council (NERC) UK-IODP programme under the grand NEB1782. Y.M. Martos thanks National

Science Foundation (NSF) subaward 97 (GG009393) for supporting her research. M.E. Weber was supported by the Deutsche Forschungsgemeinschaft (DFG grant numbers We2039/8-1 and We 2039/17-1). M. García's research was funded by the project TALUS (CGL2015-74216-JIN). T. Williams acknowledges financial support from the IODP JRSO (NSF grant number 1326927). L. Armbrecht acknowledges the Australia-New Zealand IODP Consortium (ANZIC) support. I. Bailey's research was funded by the NERC UK-IODP grant NE/T006609/1 and EU MARINEFF project (Interreg VA France-(Channel)-England Programme project #162). F.S. Hoem acknowledges funding through NWO Netherlands Polar Programme grant ALW.2016.001. The U.S. members of IODP Expedition 382 acknowledge the support by the NSF-funded U.S. Science Support Program based at Columbia University award OCE 1450528. This research used data provided by the International Ocean Discovery Program (IODP). Our acknowledgement is extended to the Spanish Antarctic Science Program that has funded geophysical and geological data acquisition within the project grants CTM2011-30241-C2-1/2 and CTM2014-60451-C2-1/2 providing part of the pre-site survey data for the IODP Expedition 382. Our heartfelt acknowledgement to the captain, crew and technicians of *JOIDES Resolution* who made a successful expedition possible. We further thank Karsten Gohl and an anonymous reviewer whose constructive comments on the initial manuscript have contributed greatly to this final version.

Appendix A. Supplementary material

Supplementary material related to this article can be found online at https://doi.org/10.1016/j.epsl.2020.116657.

References

Anderson, J.B., Warny, S., Askin, R.A., Wellner, J.S., Bohaty, S.M., Kirshner, A.E., Livsey, D.N., Simms, A.R., Smith, T.R., Ehrmann, W., Lawver, L.A., Barbeau, D., Wise, S.W., Kulhenek, D.K., Weaver, F.M., Majewski, W., 2011. Progressive Cenozoic cooling and the demise of Antarctica's last refugium. Proc. Natl. Acad. Sci. USA 108, 11356–11360.

Barker, P.F., Filippelli, G.M., Florindo, F., Martin, E.E., Scher, H.D., 2007. Onset and role of the Antarctic circumpolar current. Deep-Sea Res., Part 2, Top. Stud. Oceanogr. 54, 2388–2398.

Barth, A.M., Clark, P.U., Bill, N.S., He, F., Pisias, N.G., 2018. Climate evolution across the mid-brunhes transition. Clim. Past 14, 2071–2087.

Bijl, P.K., Bendle, J.A., Bohaty, S.M., Pross, J., Schouten, S., Tauxe, L., Stickley, C.E., McKay, R.M., Rohl, U., Olney, M., Sluijs, A., Escutia, C., Brinkhuis, H., Expedition, S., 2013. Eocene cooling linked to early flow across the Tasmanian gateway. Proc. Natl. Acad. Sci. USA 110, 9645–9650.

Bohoyo, F., Galindo-Zaldívar, J., Jabaloy, A., Maldonado, A., Rodríguez-Fernández, J., Schreider, A., Suriñach, E., 2007. Extensional deformation and development of deep basins associated with the sinistral transcurrent fault zone of the Scotia–Antarctic plate boundary. In: Cunningham, W.D., Mann, P. (Eds.), Tectonics of Strike-Slip Restraining and Releasing Bends. Geological Society, London, pp. 203–217. Special Publications.

Carter, L., McCave, I.N., 1994. Development of sediment drifts approaching an active plate margin under the SW Pacific deep western boundary current. Paleoceanography 9, 1061–1085.

Dalziel, I.W.D., Lawver, L.A., Pearce, J.A., Barker, P.F., Hastie, A.R., Barfod, D.N., Schenke, H.W., Davis, M.B., 2013. A potential barrier to deep Antarctic circumpolar flow until the late Miocene? Geology 41, 947–950.

De Vleeschouwer, D., Vahlenkamp, M., Crucifix, M., Pälike, H., 2017. Alternating Southern and Northern Hemisphere climate response to astronomical forcing during the past 35 m.y. Geology 45, 375–378.

Diekmann, B., Kuhn, G., Gersonde, R., Mackensen, A., 2004. Middle Eocene to early Miocene environmental changes in the sub-Antarctic Southern Ocean: evidence from biogenic and terrigenous depositional patterns at ODP site 1090. Glob. Planet. Change 40, 295–313.

Doherty, J.M., Thibodeau, B., 2018. Cold water in a warm world: investigating the origin of the Nordic Seas' unique surface properties during MIS 11. Front. Mar. Sci. 5.

Eagles, G., Jokat, W., 2014. Tectonic reconstructions for paleobathymetry in Drake Passage. Tectonophysics 611, 28–50.

Eagles, G., Livermore, R., Morris, P., 2006. Small basins in the Scotia Sea: the Eocene Drake Passage gateway. Earth Planet. Sci. Lett. 242, 343–353.

Galindo-Zaldívar, J., Bohoyo, F., Maldonado, A., Schreider, A., Suriñach, E., Vázquez, J.T., 2006. Propagating rift during the opening of a small oceanic basin: the Protector Basin (Scotia Arc, Antarctica). Earth Planet. Sci. Lett. 241, 398–412.

Galindo-Zaldívar, J., Puga, E., Bohoyo, F., González, F.J., Maldonado, A., Martos, Y.M., Pérez, L.F., Ruano, P., Schreider, A.A., Somoza, L., Suriñach, E., Díaz de Federico, A., 2014. Magmatism, structure and age of Dove Basin (Antarctica): a key to understanding South Scotia Arc development. Glob. Planet. Change 122, 50–69.

Gersonde, R., Abelmann, A., Burckle, L.H., Hamilton, N., Lazarus, D., McCartney, K., O'Brien, P., Spieß, V., Wise, S.W.J., 1990. Biostratigraphic synthesis of Neogene siliceous microfossils from the Antarctic Ocean, ODP LEG 113 (Weddell Sea). In: Barker, P.F., Kennett, J.P., et al. (Eds.), Proceedings of the Ocean Drilling Program Volume 113, Scientific Results. Sites 689-697. Ocean Drilling Program. College Station, Texas, pp. 915–936.

Gradstein, F.M., Ogg, J.G., Schmitz, M.D., Ogg, G.M., 2012. The Geologic Time Scale. Elsevier, Oxford.

Hatfield, R.G., Reyes, A.V., Stoner, J.S., Carlson, A.E., Beard, B.L., Winsor, K., Welke, B., 2016. Interglacial responses of the southern Greenland ice sheet over the last 430,000 years determined using particle-size specific magnetic and isotopic tracers. Earth Planet. Sci. Lett. 454, 225–236.

Herbert, T.D., Lawrence, K.T., Tzanova, A., Peterson, L.C., Caballero-Gill, R., Kelly, C.S., 2016. Late Miocene global cooling and the rise of modern ecosystems. Nat. Geosci. 9, 843–847.

Herbert, T.D., Ng, G., Cleaveland Peterson, L., 2015. Evolution of Mediterranean Sea surface temperatures 3.5–1.5 Ma: regional and hemispheric influences. Earth Planet. Sci. Lett. 409, 307–318.

Hernández-Molina, F.J., Larter, R.D., Rebesco, M., Maldonado, A., 2006. Miocene reversal of bottom water flow along the Pacific Margin of the Antarctic Peninsula: stratigraphic evidence from a contourite sedimentary tail. Mar. Geol. 228, 93–116.

Huang, H., Gutjahr, M., Eisenhauer, A., Kuhn, G., 2020. No detectable Weddell Sea Antarctic bottom water export during the last and penultimate glacial maximum. Nat. Commun. 11, 424.

Karas, C., Nurnberg, D., Bahr, A., Groeneveld, J., Herrle, J.O., Tiedemann, R., deMenocal, P.B., 2017. Pliocene oceanic seaways and global climate. Sci. Rep. 7, 39842.

Kwiek, P.B., Ravelo, A.C., 1999. Pacific Ocean intermediate and deep water circulation during the Pliocene. Palaeogeogr. Palaeoclimatol. Palaeoecol. 154, 191–217.

Larter, R.D., Vanneste, L.E., Morris, P., Smythe, D.K., 2003. Structure and tectonic evolution of the South Sandwich arc. In: Larter, R.D., Leat, P.T. (Eds.), Intra-Oceanic Subduction Systems: Tectonic and Magmatic Processes. Geological Society, London, pp. 255–284. Special Publications, London.

Levy, R.H., Meyers, S.R., Naish, T.R., Golledge, N.R., McKay, R.M., Crampton, J.S., DeConto, R.M., De Santis, L., Florindo, F., Gasson, E.G.W., Harwood, D.M., Luyendyk, B.P., Powell, R.D., Clowes, C., Kulhanek, D.K., 2019. Antarctic ice-sheet sensitivity to obliquity forcing enhanced through ocean connections. Nat. Geosci. 12, 132–137.

Livermore, R., Eagles, G., Morris, P., Maldonado, A., 2004. Shackleton fracture zone: no barrier to early circumpolar ocean circulation. Geology 32, 797–800.

Maldonado, A., Bohoyo, F., Galindo-Zaldívar, J., Hernández-Molina, F.J., Jabaloy, A., Lobo, F.J., Rodríguez-Fernández, J., Suriñach, E., Vázquez, J.T., 2006. Ocean basins near the Scotia - Antarctic plate boundary: Influence of tectonics and paleoceanography on the Cenozoic deposits. Mar. Geophys. Res. 27 (2), 83–107.

Maldonado, A., Bohoyo, F., Galindo-Zaldívar, J., Hernández-Molina, F.J., Lobo, F.J., Lodolo, E., Martos, Y.M., Pérez, L.F., Schreider, A.A., Somoza, L., 2014. A model of oceanic development by ridge jumping: opening of the Scotia Sea. Glob. Planet. Change 123, 152–173.

Martínez-García, A., Rosell-Melé, A., McClymont, E.L., Gersonde, R., Haug, G.H., 2010. Sea surface temperature estimates and alkenone C37:4 abundances in ODP site 145-882 and 177-1090. Supplement to: Martínez-García, A., et al. (2010): Subpolar Link to the Emergence of the Modern Equatorial Pacific Cold Tongue Science 328 (5985), 1550–1553. https://doi.org/10.1126/Science.1184480.PANGAEA.

Martos, Y.M., Catalán, M., Galindo-Zaldívar, J., Maldonado, A., Bohoyo, F., 2014. Insights about the structure and evolution of the Scotia Arc from a new magnetic data compilation. Glob. Planet. Change 123, 239–248.

Martos, Y.M., Maldonado, A., Lobo, F.J., Hernández-Molina, F.J., Pérez, L.F., 2013. Tectonics and palaeoceanographic evolution recorded by contourite features in southern Drake Passage (Antarctica). Mar. Geol. 343, 76–91.

McKay, R., Naish, T., Carter, L., Riesselman, C., Dunbar, R., Sjunneskog, C., Winter, D., Sangiorgi, F., Warren, C., Pagani, M., Schouten, S., Willmott, V., Levy, R., DeConto, R., Powell, R.D., 2012. Antarctic and Southern Ocean influences on late Pliocene global cooling. Proc. Natl. Acad. Sci. USA 109, 6423–6428.

Miller, K.G., Wright, J.D., Browning, J.V., 2005. Visions of ice sheets in a greenhouse world. Mar. Geol. 217, 215–231.

Montes, C., Cardona, A., Jaramillo, C., Pardo, A., Silva, J.C., Valencia, V., Ayala, C., Pérez-Angel, L.C., Rodriguez-Parra, L.A., Ramirez, V., Niño, H., 2015. Middle Miocene closure of the Central American Seaway. Science 348, 226–229.

Naveira-Garabato, A.C., McDonagh, E.L., Stevens, D.P., Heywood, K.J., Sanders, R.J., 2002. On the export of Antarctic bottom water from the Weddell Sea. Deep-Sea Res., Part 2, Top. Stud. Oceanogr. 49, 4715–4742.

O'Dea, A., Lessios, H.A., Coates, A.G., Eytan, R.I., Restrepo-Moreno, S.A., Cione, A.L., Collins, L.S., de Queiroz, A., Farris, D.W., Norris, R.D., Stallard, R.F., Woodburne,

M.O., Aguilera, O., Aubry, M.-P., Berggren, W.A., Budd, A.F., Cozzuol, M.A., Coppard, S.E., Duque-Caro, H., Finnegan, S., Gasparini, G.M., Grossman, E.L., Johnson, K.G., Keigwin, L.D., Knowlton, N., Leigh, E.G., Leonard-Pingel, J.S., Marko, P.B., Pyenson, N.D., Rachello-Dolmen, P.G., Soibelzon, E., Soibelzon, L., Todd, J.A., Vermeij, G.J., Jackson, J.B.C., 2016. Formation of the Isthmus of Panama. Sci. Adv. 2, e1600883.

Pérez, L.F., Hernández-Molina, F.J., Lodolo, E., Bohoyo, F., Galindo-Zaldívar, J., Maldonado, A., 2019. Oceanographic and climatic consequences of the tectonic evolution of the southern scotia sea basins, Antarctica. Earth-Sci. Rev. 198, 102922.

Pérez, L.F., Maldonado, A., Bohoyo, F., Hernández-Molina, F.J., Vázquez, J.T., Lobo, F.J., Martos, Y.M., 2014. Depositional processes and growth patterns of isolated oceanic basins: the Protector and Pirie basins of the Southern Scotia Sea (Antarctica). Mar. Geol. 357, 163–181.

Pérez, L.F., Maldonado, A., Hernández-Molina, F.J., Lodolo, E., Bohoyo, F., Galindo-Zaldívar, J., 2017. Tectonic and oceanographic control of sedimentary patterns in a small oceanic basin: Dove Basin (Scotia Sea, Antarctica). Basin Res. 29, 255–276.

Pollard, D., DeConto, R.M., 2009. Modelling West Antarctic ice sheet growth and collapse through the past five million years. Nature 458, 329–332.

Raymo, M.E., Mitrovica, J.X., 2012. Collapse of polar ice sheets during the stage 11 interglacial. Nature 483, 453–456.

Rohling, E.J., Foster, G.L., Grant, K.M., Marino, G., Roberts, A.P., Tamisiea, M.E., Williams, F., 2014. Sea-level and deep-sea-temperature variability over the past 5.3 million years. Nature 508, 477–482.

Ryan, W.B.F., Carbotte, S.M., Coplan, J.O., O'Hara, S., Melkonian, A., Arko, R., Weissel, R.A., Ferrini, V., Goodwillie, A., Nitsche, F., Bonczkowski, J., Zemsky, R., 2009. Global multi-resolution topography synthesis. Geochem. Geophys. Geosyst. 10.

Scher, H.D., Martin, E.E., 2006. Timing and climatic consequences of the opening of drake passage. Science 312, 428–430.

Sijp, W.P., England, M.H., 2004. Effect of the drake passage throughflow on global climate. J. Phys. Oceanogr. 34, 1254–1266.

Torres-Carbonell, P.J., Dimieri, L.V., Olivero, E.B., Bohoyo, F., Galindo-Zaldívar, J., 2014. Structure and tectonic evolution of the Fuegian Andes (southernmost South America) in the framework of the Scotia Arc development. Glob. Planet. Change.

van Wijk, J.W., Lawrence, J.F., Driscoll, N.W., 2008. Formation of the Transantarctic Mountains related to extension of the West Antarctic Rift system. Tectonophysics 458, 117–126.

Weber, M.E., Raymo, M.E., Peck, V.L., Williams, T., IODP Expedition 382 Scientists, 2021. Iceberg Alley and Subantarctic Ice and Ocean Dynamics. Proceedings of the International Ocean Discovery Program, 382: College Station, TX (International Ocean Discovery Program). https://doi.org/10.14379/diop.proc.382.2021.

Wilson, D.J., Bertram, R.A., Needham, E.F., van de Flierdt, T., Welsh, K.J., McKay, R.M., Mazumder, A., Riesselman, C.R., Jimenez-Espejo, F.J., Escutia, C., 2018. Ice loss from the East Antarctic ice sheet during late Pleistocene interglacials. Nature 561, 383–386.